Published in IET Radar, Sonar and Navigation
Received on 31st October 2011
Revised on 4th February 2012
doi: 10.1049/iet-rsn.2011.0352

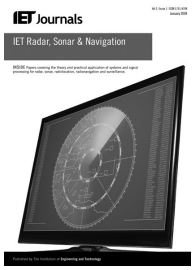

ISSN 1751-8784

Ultra wideband indoor navigation system

M. Segura[1,2] *V. Mut*[1,2] *C. Sisterna*[1,3]

[1]*Avenida Libertador 1109 oeste, CP5400 San Juan, San Juan City, Argentina*
[2]*Automatics Institute, National University of San Juan, San Juan City, Argentina*
[3]*Electronics Department, National University of San Juan, San Juan City, Argentina*
E-mail: msegura@unsj.edu.ar

Abstract: Typical indoor environments contain multiple walls and obstacles consisting of different materials. As a result, current narrowband radio frequency (RF) indoor navigation systems cannot satisfy the challenging demands for most indoor applications. The RF ultra wideband (UWB) system is a promising technology for indoor localisation owing to its high bandwidth that permits mitigation of the multipath identification problem. This work proposes a novel UWB navigation system that permits accurate mobile robot (MR) navigation in indoor environments. The navigation system is composed of two sub-systems: the localisation system and the MR control system. The main contributions of this work are focused on estimation algorithm for localisation, digital implementation of transmitter and receiver and integration of both sub-systems that enable autonomous robot navigation. For sub-systems performance evaluation, statics and dynamics experiments were carried out which demonstrated that the proposed system reached an accuracy that outperforms traditional sensors technologies used in robot navigation, such as odometer and sonar.

1 Introduction

This paper addresses the design of an ultra wideband (UWB) navigation system that allows mobile robot (MR) or another mobile vehicle autonomous navigation in indoor environments. The experimental results show that the proposed system is suitable for MR applications.

The radio frequency (RF) localisation using UWB signals is a promising technology for indoor localisation because of its high bandwidth which permits multipath identification in indoor environments, one of the main problems in indoor communication channels. Although it has been used in military applications for 50 years, UWB has recently gained attention among researchers as well as in industry.

Indoor applications have significantly higher demands concerning localisation accuracy, cost and update rate than most outdoor applications. Owing to that, hardly any existing outdoor solution operates satisfactorily in the cluttered indoor environment. Hence, new indoor localisation techniques are needed under low-cost, low-power and high-accuracy conditions.

Based on the best knowledge to date, a limited number of UWB architectures have been proposed in the bibliography consulted for MR indoor navigation. In the field of MR, navigation describes the technique that allows a robot to use information it has gathered about the environment to reach goals that are established a priori.

In [1], a multi-cell impulse radio UWB system was evaluated. The MR transmits UWB signals and the receivers are ceiling-mounted. The position estimation is fed back to a MR using a ZigBee transceiver. In [2], a UWB commercial localisation system from PulseOn [3] and a GPS receiver were mounted on the MR. Combined indoor and outdoor experiments using fusion techniques were carried out. This system shows good results, but it cannot be considered as a UWB navigation system because the robot navigates using an odometer and a laser sensor. In [4], UWB localisation combined with odometry was proposed for MR tracking in different indoor environments, using the concept of self-localisation since the MR is equipped with a UWB receiver. However, it does not integrate the control and localisation UWB systems.

Different requirements must be satisfied by an indoor localisation system that assists MR navigation. Accuracy is the most important in this application, because in real scenarios MR requires 20 cm navigation accuracy 90% of the time, at least. Considering typical indoor office environments the localisation system coverage must be approximately 20 m^2 or bigger. The system must allow multiple users; therefore some type of diversity should be evaluated. The system must work properly under line-of-sight or non-line-of-sight (LOS/NLOS) conditions. Finally, the developed prototype must allow high degree of reconfiguration and flexibility.

One of the most significant impairments in indoor accurate navigation is the NLOS problem that takes place when there is no direct link between the transmitter and the receiver. Different NLOS error mitigation techniques have been proposed in the bibliography [5–9]. This work proposes a novel dynamic threshold crossing algorithm that detects the first arrival signal in LOS/NLOS situations and estimates the time of arrival (TOA); for a detailed algorithm description see [10].

In the work described in this paper, the UWB signal robustness against ambient conditions and the channel

propagation characteristics were evaluated through a measurement campaign in indoor office environment. Furthermore, this paper presents the integration of a UWB localisation system with a control system for MR. A comparative analysis between classical odometry navigation and the proposed UWB navigation is presented, showing the advantages of the developed system. The experimental analysis includes a complete statistical evaluation, navigation accuracy and comparative performance.

The paper is organised as follows: Section 2 details the complete system description that includes indoor communication channel characteristics, transmitter and receiver design; Section 3 describes the indoor localisation system, which consists of two steps: TOA estimation and ranging estimation; Section 4 describes the statistical experiments results and the covariance analysis; Section 5 introduces the MR principal characteristics and details the localisation system embedded into the control loop; finally, Section 6 details the conclusions.

2 System description

There are three components that constitute a localisation system using RF signals: the domain, the environment and the methodology [11]. In this work, a custom Cartesian coordinate system with reference at the lower-left corner environment map is used. The proposed environment is a typical ground indoor office. Finally, the position is estimated using time-difference-of-arrival (TDOA) methodology.

Localisation using RF signals can be modelled as a system with three fundamental elements: transmitter, receiver and propagation channel. This work proposes a centralised transmitter that sends synchronised signals to fixed antennas with known positions in the indoor environment (Fig. 1). The receiver, mounted on the MR acquires the transmitted signals that travel through the indoor channel and estimates the robot position. The position estimation rate determines system tracking capabilities and maximum robot navigation speed, in this work 1 m/s. The channel characteristics will determine the UWB signal design and the signal processing complexity.

2.1 UWB indoor communication channel

Understanding the UWB communication channel is a fundamental issue for developing a navigation system because of the inherent relation between position accuracy and channel characteristics.

The earliest work done in [12] attempted to characterise the indoor channel through a measuring campaign in several indoor environments. After that, diverse research projects tried to characterise the indoor UWB channel following similar approaches as in [13]. Finally, the IEEE proposed the use of a standardised channel model for UWB communication detailed in [14]. The standardised indoor

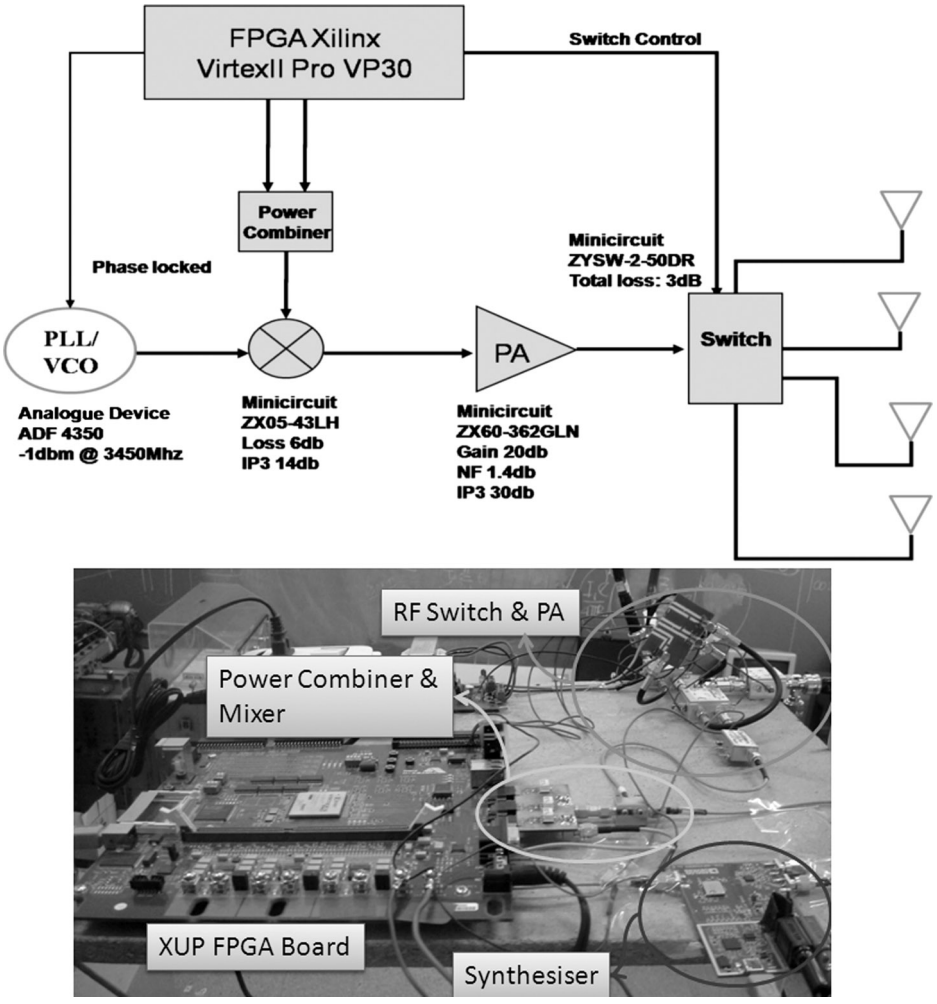

Fig. 1 *Centralised UWB digital transmitter block diagram and real implementation*

doi: 10.1049/iet-rsn.2011.0352

channel impulse response is described as follows

$$h(t) = X \sum_{l=0}^{L} \sum_{k=0}^{K} \alpha_{k,l} \delta(t - T_l - \tau_{k,l}) \quad (1)$$

In (1), X is a log−normal random variable, L is the number of arriving clusters, K is the number of paths that arrive within the l cluster, $\alpha_{k,l}$ is the amplitude of path k in cluster l, T_l is the arrival time of the cluster l and $\tau_{k,l}$ is the arrival time of path k within cluster l. The statistical characterisation for different UWB channels can be found in [14].

From the localisation point of view, the most important parameter is related to the first arriving component detection. The time-related localisation techniques estimate the absolute delay of the first arriving multipath component (MPC). This task can be easily achieved if the first MPC is the strongest. However, diffraction and reflection effects change the MPC amplitude; consequently, they are modelled as log-normal variable.

In this work, a TOA methodology is implemented in order to estimate the signal propagation delay between transmitters and receiver, as will be explained in Section 3. The channel delay spread is directly related to the number of detectable paths at the receiver side and determines the maximum pulse rate for avoiding inter-pulse interference. For UWB signal model, this parameter must be estimated. In order to estimate the channel delay spread and the number of detectable MPCs, experiments were carried out at the facilities of the University of Southern California, in the Department of Electrical Engineering. On the transmitter side, 2 ns wide pulses were emitted by a horn antenna connected to a UWB transmitter. On the receiver side the signal is acquired by a digital storage oscilloscope running at 25 Gsps. The acquired signal is processed off-line for channel characterisation.

These experiments demonstrate that under LOS conditions, the received signal power is inversely proportional to the distance squared. However, some measurements near metallic doors or windows indicate that the received signal was severely attenuated and the first arriving path was not the most powerful, because of destructive interference. The LOS measurements performed near metallic structures presented strong MPC within 50 ns window, after the first arrival path. On the other hand, the LOS measurements at distances below 5 m had appreciable MPC only within the first 30 ns.

In the NLOS case, the maximum measured delay spread was 100 ns. In the presence of metallic structures, the received signal amplitude is strongly attenuated and it is difficult to differentiate the first arriving path. In NLOS, the maximum range at which the signal can be detected was approximately 7 m considering the Euclidian distance between the TX and RX, through dry walls. For LOS case, the maximum range at which the first arriving path could be detected was nearly 19 m.

Considering experiment results, a simplified model derived from the standard IEEE channel with only one cluster, $L = 1$, was adopted in this work. This simplified channel model is expressed in (2).

$$h(t) = X \sum_{k=0}^{K} \alpha_k \delta(t - \tau_k) \quad (2)$$

Considering that the worst measured NLOS delay spread was around 100 ns, a protection gap of 20% was considered to avoid inter-pulse interference.

2.2 Transmitter description

The centralised transmitter generates baseband 2 ns UWB pulses having a −10 dB bandwidth of approximately 1 GHz. These pulses are then up-converted to a centre frequency of 3.5 Ghz using a local oscillator (LO) following the proposed methodology in [15, 16]. The up-conversion architecture offers more flexibility and control over direct pulse generation at the expense of extra complexity and power consumption because of the LO circuitry. Baseband pulses are generated using a field programmable gate array (FPGA) and then are frequency up-converted using a passive mixer and a frequency synthesiser. The centre frequency and bandwidth are set by the frequency synthesiser and the baseband pulse shapes, respectively, for satisfying current regulations.

In order to meet the multiuser requirement, the receiver must identify the multiple arriving signals from transmitters. Each transmitter has a unique code that permits to differentiate its signal from others. The FPGA generate differential sequences using gold codes of length seven. The next step consists in modulating the coded pulses. In this work, a non-coherent communication system is adopted using differential binary phase shift keying (DBPSK) modulation. The transmitted signal $s(t)$, before time multiplexing, is expressed in (3), where $\tilde{b}(k) = b(k) \oplus \tilde{b}(k-1)$ are differential encoded pulses with $\tilde{b}(k) \in \{0, 1\}$, $\oplus$ represents the XOR operation, E_b is the bit energy and $p(t)$ is the selected pulse shape.

$$s(t) = \sqrt{E_b} \sum_{k=-\infty}^{+\infty} (2\tilde{b}(k) - 1) p(t - kT_f) \quad (3)$$

With the aim of avoiding multi-user interference time division multiple access (TDMA) being implemented. In the proposed architecture, TDMA is implemented using an RF switch that sends synchronised pulses to each antenna. The transmission slot length is equal to the signal symbol period defined as T_s; therefore during each slot the transmitter radiates a complete coded symbol.

The signal transmitted by each antenna can be derived from (3) considering the pulse codification and TDMA. The transmitted signal is expressed in (4), where $u = \{0, 1, \ldots, N_{\mathrm{BS}} - 1\}$, N_{BS} is the number of base stations or transmitting antennas, T_{f} is the frame time or pulse period, N_{f} is the number of frames that are equivalent to the code length and $C_{\mathrm{u\_DS}}(k)$ is the DBPSK signal codified by the direct sequence code assigned to each antenna.

$$s_{\mathrm{u\_DS}}(t) = N_{\mathrm{f}} \sqrt{E_b} \sum_{k=0}^{N_{\mathrm{f}}-1} C_{\mathrm{u\_DS}}(k) p(t - kT_{\mathrm{f}} - uT_{\mathrm{s}}) \quad (4)$$

As shown in Fig. 1, the transmitter is a modular system implemented with commercial off-the-shelf components. The transmitter characteristics such as bandwidth, modulation, centre frequency, pulse rate, power, codification and TDMA can be changed with minor effort, thanks to system flexibility and reconfiguration capabilities. This is an advantage of the developed prototype against other designs.

2.3 Receiver description

In this work, the reconfiguration and flexibility capabilities were an important requirement. To accomplish this requirement on the receiver side, the software-defined radio concept is applied, where reconfiguration and flexibility are

provided by FPGA board. The receiver characteristics and processing algorithms can be changed by downloading a different bit stream to the FPGA, this gives high degree of flexibility and accelerates the design process. The proposed receiver can be classified as a non-coherent all digital energy detector since the received signal is first down-converted and then sampled using high-speed ADC. The operations performed in the analogue domain are down-conversion, filtering and amplification, as Fig. 2 shows; the following signal processing is implemented on the digital domain.

Considering that DBPSK was used for modulation, it is necessary to compare the phases of two consecutive pulses for demodulation. Therefore the receiver needs to generate a delay equal to T_f. The accuracy of the receiver is related to the capacity to produce a precise delay. Since it is difficult to make an accurate analogue delay, received signals are directly digitised and the delay is performed on the digital domain. The received signal $r(t)$ is correlated with a delayed signal coming from the same transmitter in the digital domain. This correlation improves the signal-to-noise-ratio (SNR) because the transmitted signals are scattered by the same objects and modified by the same communication channel; therefore they are highly correlated.

The receiver is implemented by a dual 8-bit ADC that runs at 1.5 Gsps and a Virtex4 Xilinx FPGA for signal processing. The advantage of this receiver is that phase recovery and frequency recovery are not needed because of the non-coherent characteristic. The block diagram of the differential receiver is shown in Fig. 2, for more details see [17, 18].

3 Indoor localisation system

The current work is based on absolute self-positioning localisation with a two-step technique. The absolute localisation system determines the position of the MR referred to fixed reference points with known locations. The localisation algorithm is classified as a 'two step positioning system'. In the first step the algorithm estimates the signal TOA, then in the second step, the position is estimated using a TDOA and a hyperbolic geometric technique. The proposed system can be considered as radio detection and ranging, because in the first step the system detects a radio signal and estimates the TOA. Then, in the second step, the position is estimated based on ranging estimation and adequate positioning algorithms.

3.1 First step: TOA estimation algorithm

Several ideas have been proposed in the bibliography, which attempt to solve the most significant problems presented in TOA estimation of UWB signal in indoor environments. The achievable accuracy depends on clock synchronisation between the transmitter and the receiver. In this work the synchronisation is made by a centralised transmitter that implements TDMA and therefore no synchronisation is required on the receiver side.

The proposed threshold-based TOA algorithm selects the time at which the signal Y_D at the detector output crosses an established threshold (Fig. 3). The estimation accuracy depends on the threshold selection. If the threshold is low, the probability of detecting a peak because of noise increases. This leads to either false alarm or early detection. On the other hand, if the threshold is high, the probability of detecting a signal that arrives later than the direct path increases, therefore late detection can occur.

Accurate TOA estimation requires time delay estimation techniques that provide resistance to noise and interference and the ability to resolve multipath signal components. In previous works by the authors [10, 19], simple, robust and efficient TOA estimation algorithm has been developed.

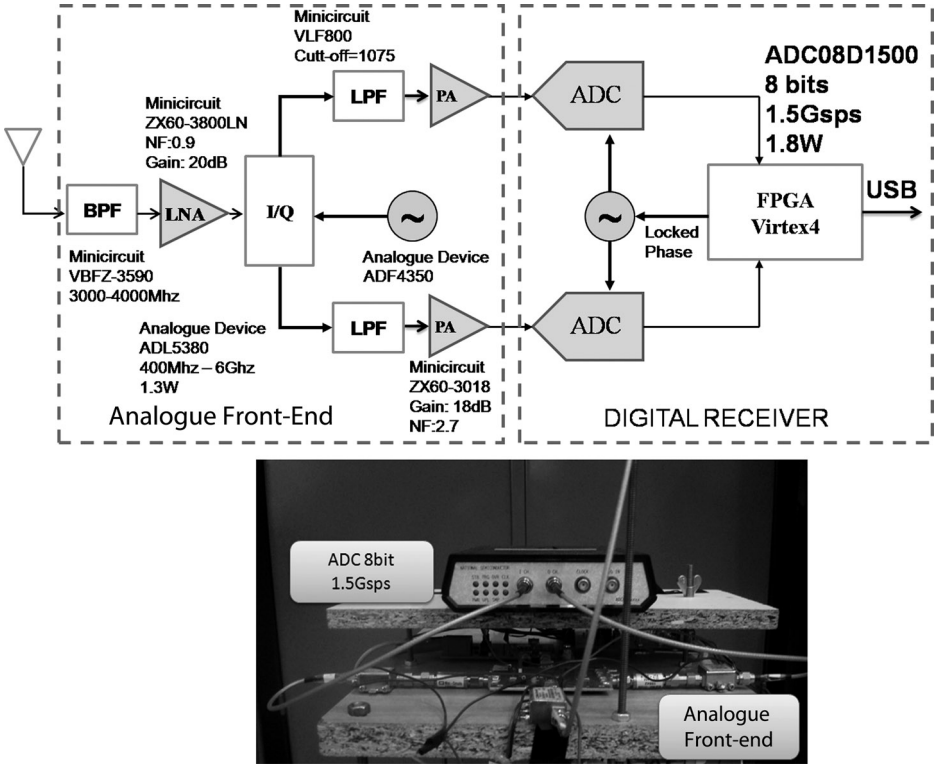

Fig. 2 *Digital receiver block diagram and real implementation*

doi: 10.1049/iet-rsn.2011.0352

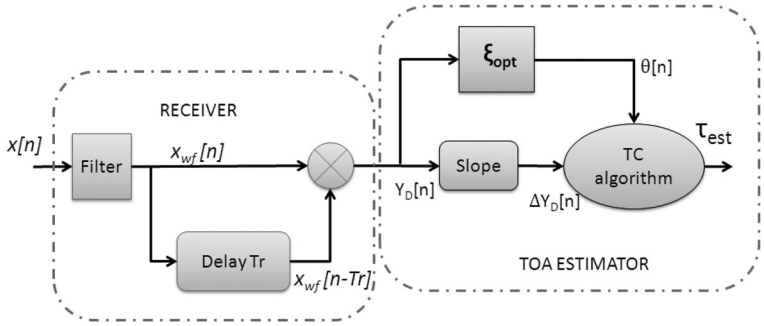

Fig. 3 *Receiver structure and dynamic threshold crossing algorithm*

The proposed TOA estimator is an adaptive threshold crossing algorithm based on cyclic cross correlation and wavelet filter theory. The dynamic threshold is calculated as the root mean square (RMS) of cross-correlated signal $Y_D[n]$ at the receiver output (5). This RMS is calculated over a sliding window of length T_{w_th}; therefore the threshold is updated at every sample time. The main advantage of the proposed algorithm is that only one parameter, T_{w_th}, must be optimised for proper threshold selection. This window length is directly related to channel delay spread, which was estimated in Section 2.1.

$$\theta[n] = \mathrm{RMS}(Y_D[n]) = \sqrt{\frac{1}{T_{w_{th}}} \sum_{i=n-T_{w_{th}}}^{n} Y_D[n]^2} \quad (5)$$

The complete receiver and TOA estimator block diagram are shown in Fig. 3. The block called ξ_{opt}, determines the optimum threshold solving (5) each sample time.

The threshold crossing algorithm evaluates the receiver output $Y_D[n]$ slope and detects the first arriving path when slope $\Delta Y_D[n]$ defined in (6) is greater than the estimated $\theta[n]$ threshold.

$$\Delta Y_D = Y_D(k+2) - Y_D(k) \quad (6)$$

The decision principle is summarised in (7).

$$\hat{\tau} = \{n | \Delta Y_D[n] > \theta[n]\} \quad (7)$$

Finally, at the output of the TOA estimator block, an estimated BPSK sequence is generated considering the $\hat{\tau}$ values. In order to identify the multiple sequences from transmitters a sliding correlation operation is performed between the estimated sequence $\hat{b}(k)$ and each transmitter gold sequence. This cross-correlation is performed at the TOA estimator block and determines the signal delay from each transmitter.

3.2 Second step: ranging algorithm

The TDOA ranging method does not require the knowledge of transmission absolute time; therefore with estimated TOA it is possible to calculate the TDOA considering one transmitter as a reference. If there is some timing bias on the transmitted signals the difference operation allows its cancellation when the biases are similar.

The MR estimates the ranges between transmitters and its current position multiplying the estimated time difference with the electromagnetic wave propagation speed. These ranges produce a set of hyperbolas and its intersection determine the MR position (8). In a 2-D position localisation system, the transmitter position is expressed as (X_{tx}, Y_{tx}), the MR location is expressed as (x_{MR}, y_{MR}) and the range is calculated as

$$R_i = \sqrt{(X_{tx} - x_{MR})^2 + (Y_{tx} - y_{MR})^2} \quad (8)$$

The range difference between transmitters is expressed in (9), where c is the electromagnetic wave propagation speed and $\tau_{i,1}$ is the TDOA estimation between Tx '1' and Tx 'i'.

$$R_{i,1} = c.\tau_{i,1} = R_i - R_1 \quad (9)$$

Classical techniques for solving (9) include the least squares and weighted least squares methods. For moderate or large measurement noise, the approximations used on these techniques may not be valid and will lead to degraded estimation performance. Therefore in this work the ranging algorithm proposed in [20] is implemented because it reduces the mentioned problem.

4 Statistical error analysis

In this section, static measurements were taken from known positions and were evaluated using different error probability tests in order to determine the algorithm deviations and accuracy.

The ellipse error analysis is a multidimensional measure of accuracy for an unbiased estimator. If the position in a 2-D localisation system is defined as vector $\boldsymbol{x}$ that contains both coordinates, the range measurement can be defined as a function of the position plus the noise measurement as expressed in (10).

$$\boldsymbol{r} = f(\boldsymbol{x}) + \boldsymbol{n} \quad (10)$$

Following the equations expressed in [21] for ellipse error measurement, the covariance matrix of the estimated measure $\boldsymbol{x}$ for the 2-D case can be written as shown in (11).

$$\mathbb{P} = \begin{bmatrix} \sigma_x^2 & \sigma_{xy}^2 \\ \sigma_{yx}^2 & \sigma_y^2 \end{bmatrix} \quad (11)$$

If $\sigma_{xy} = \sigma_{yx} = 0$ then it is possible to approximate $\lambda_x = \sigma_x^2$ and $\lambda_y = \sigma_y^2$, following these approximations, the major and minor ellipse axis can be calculated as: $2\sqrt{k\lambda_x}$, $2\sqrt{k\lambda_y}$, respectively, for more details see [21].

The statistical experiments were performed in our Telecommunication Laboratory. Figs. 4*a* and *b* show an

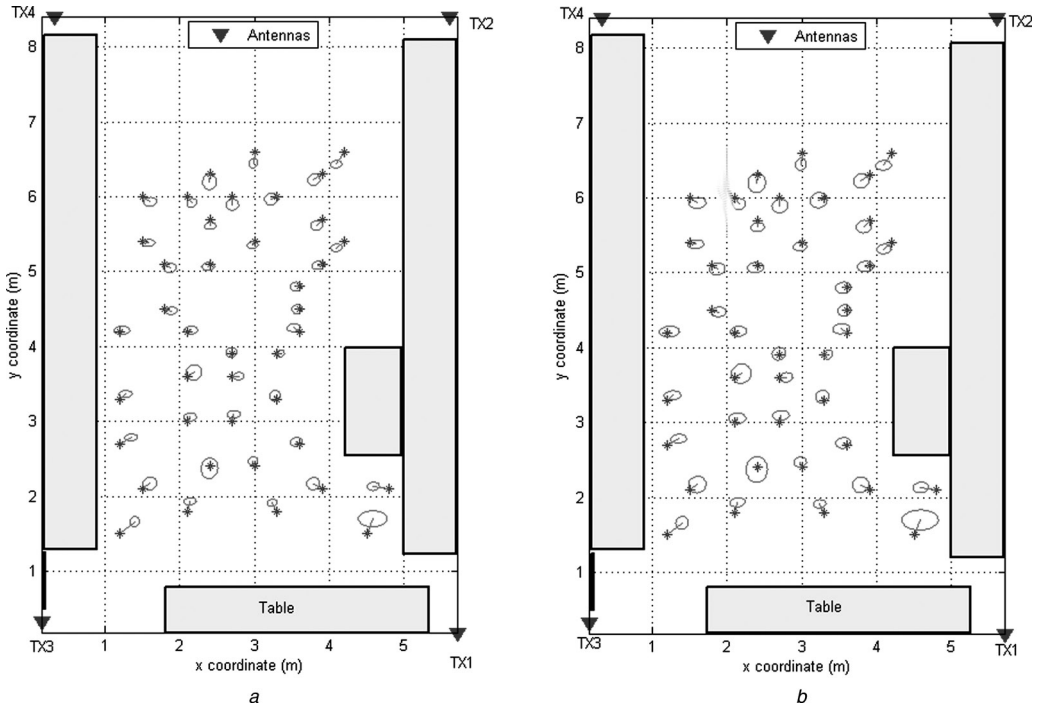

Fig. 4 *Ellipse error probability*

a Shows the ellipse error probability of 50%
b Shows the ellipse error probability of 67%

approximated floor map. All TX antennas are located at the same height of 2.45 m in the lab corners. The RX antenna is mounted over the MR with a height of 0.82 m.

Two ellipse tests were performed, one considering a probability error of 50% and the other with 67% probability error. These values are commonly used for characterising the accuracy of localisation systems. The 50% probability error is considered as the circular error probability (CEP) measurement where the ellipse has equal axis. The 67% probability error is considered an approximation to the standard deviation σ in a Gaussian distribution.

The experiments were completed over 41 known positions. The positions were measured with an accuracy of ± 1 cm. On each position 50 measurements were performed. The statistical error results of previously mentioned experiments are shown in Figs. 4*a* and *b*. The black triangles are the positions of Disc-cone UWB antennas. The grey rectangles are work tables with shelves mounted on the top and the lab door is in the lower-left corner. The asterisks indicate the true position, and the line that interconnects this position with the ellipse centre determines the Euclidian distance. This distance can be considered as the estimator bias and the ellipse semi-axes express the estimator variance in both axes.

Evaluating Fig. 4*a*, it is possible to determine that only one position, near Tx1, has a major ellipse axis bigger than the system requirement that is 20 cm. The position error is higher than the system requirement near TX antennas, because in these locations the mesurements errors are similar to range distances, opposite to Chang's algorithm assumption [22]. However, considering the obtained results it is possible to assert that the CEP satisfies the system requirements. Considering the obtained results it is possible to assert that the CEP satisfies the system requirements.

Evaluating Fig. 4*b*, it is possible to determine that 90% of estimated positions have a standard deviation σ, below 20 cm. Furthermore, the lines that express the estimator bias are below system requirements, except in the corners near TX sites. The statistical results reveal that the proposed TOA and Ranging algorithm bring adequate accuracy and repeatability.

In order to evaluate the absolute error, the cumulative density plot (CDF) of the mean absolute errors in both coordinates were calculated as expressed in (12), where N denotes the measurements per position. In Fig. 5, the CDF in both axes were plotted.

$$\mathrm{MAE} = \frac{1}{N}\sum_{k=1}^{N} |\hat{\boldsymbol{x}} - \boldsymbol{x}| \tag{12}$$

Evaluating Fig. 5 it is possible to determine that 95% of the estimated positions in both axes have an absolute error less than 20 cm, these results outperform the simulation performed on previous authors' work [10], where 75% of simulation were below 20 cm. On the other hand, errors greater than 20 cm are more frequently on axis x. This situation takes place since the laboratory dimension on the x-axis is smaller than dimension on the y-axis hence; the transmitter separations on y dimension are larger than on x dimension. In the described scenario, the same measurement error or noise exerts greater influence on the smaller range estimation and therefore on the final position estimation.

The root mean square error (RMSE) was calculated as expressed in (13). The aim of such a test is to compare this result with the theoretical Cramer–Rao lower-bound (CRLB) value expressed in [23] and with previous simulated values expressed in [19]. If vector $\hat{\boldsymbol{x}}$ is defined as the position estimation, then the RMSE value is expressed as follows

$$\mathrm{RMSE}(\hat{\boldsymbol{x}}) = \sqrt{E(x - \hat{\boldsymbol{x}})^2}, \text{ where } \hat{\boldsymbol{x}} = \{\hat{\boldsymbol{x}}, \hat{y}\} \tag{13}$$

doi: 10.1049/iet-rsn.2011.0352

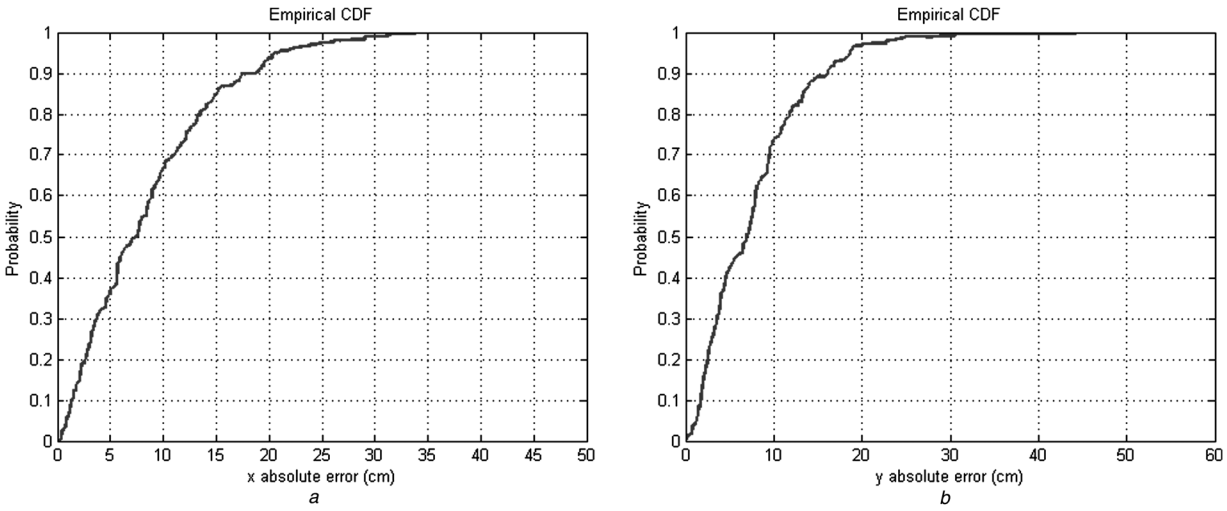

Fig. 5 *Mean absolute error CDF in coordinate x and y*

a Shows absolute error CDF in coordinate *x*
b Shows absolute error CDF in coordinate *y*

The obtained results for evaluated positions in both axes were

$$\mathrm{RMSE}(\hat{x}) = 10.83\,\mathrm{cm};\ \ \mathrm{RMSE}(\hat{y}) = 9.72\,\mathrm{cm}$$

Considering that the received signal measured at different positions generally have an SNR between -5 dB and $+5$ dB and that the transmitted pulse has a bandwidth near to 1 GHz it is possible to assert, compared with results shown in [23], that the calculated RMSE are 7 cm distance from the theoretical CRLB value. On the other hand, comparing these results with simulation in [19], it is possible to determine that experimental results improve the simulated ones. These results lead to the conclusion that developed TOA estimation in conjunction with localisation algorithm attain near-optimal estimates against the theoretical CRLB.

5 MR navigation

In this work a unicycle MR was used for experiment evaluation. This robot type can rotate freely around its axis and has two parallel driven wheels, one mounted on each side of their centre and an offset castor wheel to maintain balance.

5.1 Kinematic model and position control

Kinematic models of MRs are incorporated within the design of controllers whenever the vehicle develops tasks at low speeds and light loads, which match to the proposed experiments. MRs have quite simple mathematical models to describe their instantaneous motion capabilities.

The kinematics of MRs is expressed in (14), where u and ω are the linear and the angular velocities, respectively. The robot state variables are x, y and ψ; where (x, y) are the coordinates of the middle point between the driving wheels and ψ denotes the heading of the vehicle relative to the x-axis of the world coordinate system. The vector $[\boldsymbol{xy\psi}]^{\mathrm{T}}$ defines the posture of the vehicle.

$$\begin{cases} \dot{x} = u\cos(\psi) \\ \dot{y} = u\sin(\psi) \\ \dot{\psi} = \omega \end{cases} \tag{14}$$

The position controller in this work has predefined positions that the MR must reach. In order to reach these positions the robot uses the described kinematic model and its current estimated position to determine the suitable control actions. The robot-estimated position and orientation, ***xf***, are fed back in order to calculate the position error, ***xe***, against the desired final position, ***xd***, see Fig. 6. This error is converted to polar coordinates and the controller generates the appropriated linear velocity u and the angular velocity ω, to reach the goal. The distance error between the current and the desired position is denoted as e, and the orientation error is the difference between the desired and the current orientation $\alpha = \theta - \psi$.

5.2 Navigation experiment set-up

With the aim of evaluating the dynamic characteristics of the proposed navigation system, the UWB receiver was mounted

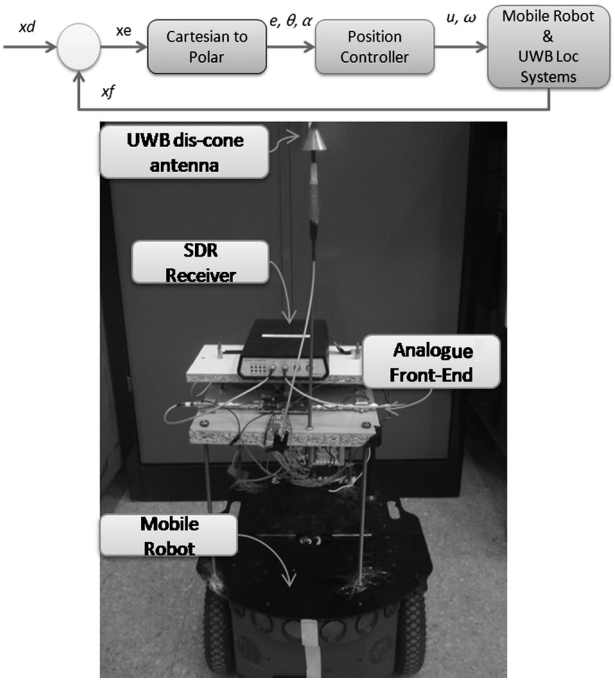

Fig. 6 *MR control system block diagram and real implementation*

Table 1 Position error at reference points, expressed in cm

	Run1		Run2		Run3		Final error	
	e_x	e_y	e_x	e_y	e_x	e_y	e_x	e_y
p1	0	0	9	13	16	17	30	18
p2	4	4	6	11	10	20		
p3	10	8	5	8	2	1.9		
p4	2	5	4	6	5	17		

on the MR. In the proposed experiment the MR navigates using the position controller described in the block diagram of Fig. 6. The experiments were performed with a Pioneer 3XD unicycle MR. The MR and the developed UWB receiver system are shown in Fig. 6.

The navigation performance using the developed UWB system was evaluated through two experiments. In the first experiment, classical odometry was used for navigation and in the second experiment the proposed UWB system was evaluated. In the second experiment, owing to the lack of orientation information, the robot uses odometry for 90° rotation once it reaches the desired position.

In this research project the navigation system is composed of the localisation and control systems. The main contribution compared against previous work is that location information is introduced into the control loop that enables a real-time navigation system. On the other hand, previous work [1, 2] requires an external system that sends the position to the MR, these approaches limit the control period which finally affect the control actions and the maximum robot speed.

5.3 Experiment results

The MR must reach four reference positions on each run. The MR started at p1(3.6,6.3) and must pass three reference positions p2(1.8,6.3), p3(1.8,2.1) and p4(3.6,2.1) before coming back to the starting position p1. The reference positions are expressed in metres for the x and y coordinates, respectively.

The first experiment using odometry was repeated three times for accumulated error analysis. The robot trajectory describes a set of rectangles where because of odometry accumulated error, the initial position differs from the final position. The position errors at each reference are expressed in cm for each run in Table 1.

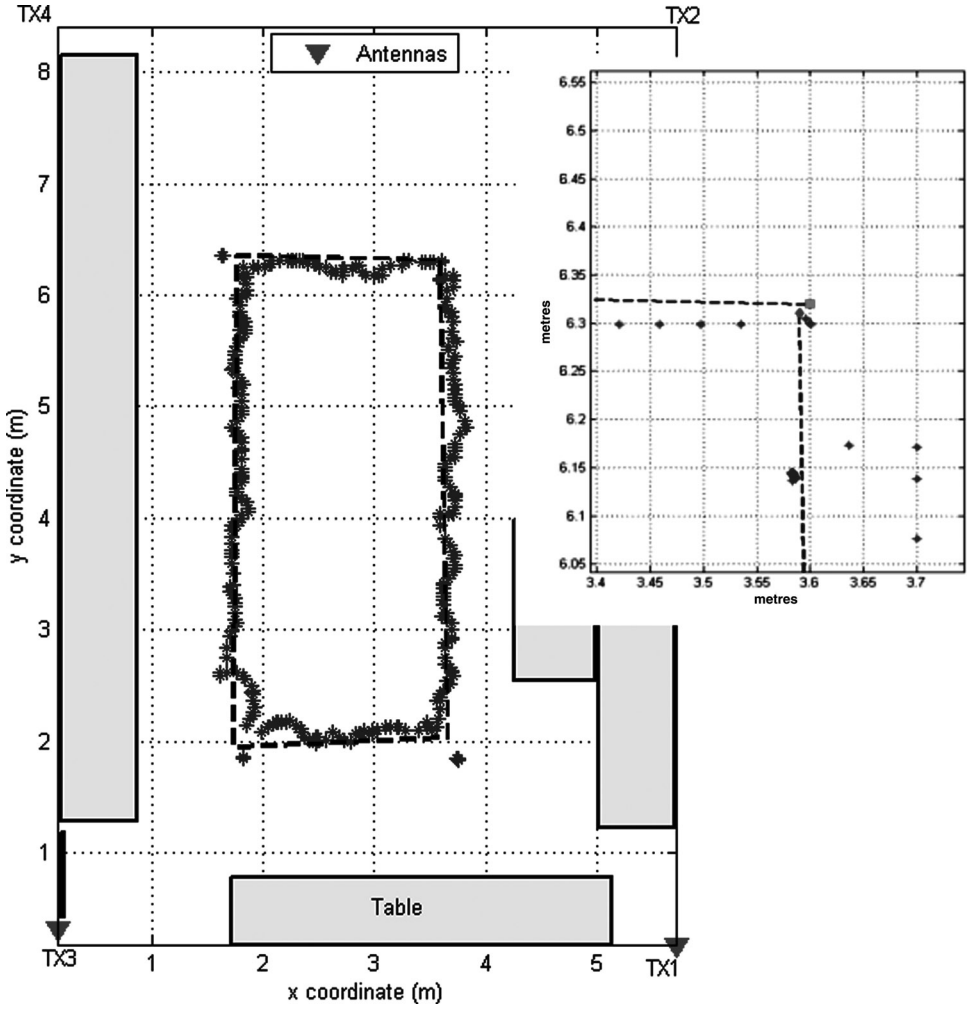

Fig. 7 *Experiment result with UWB navigation system*

doi: 10.1049/iet-rsn.2011.0352

Table 2 Position error at reference points, expressed in cm

	Run1		Run2		Run3		Final error	
	e_x	e_y	e_x	e_y	e_x	e_y	e_x	e_y
p1	0	0	8	0	1	2	1	1
p2	4	7	7	10	4	6		
p3	6	17	4	12	7	15		
p4	8	4	10	0	6	6		

In the second experiment, three runs were evaluated using UWB localisation. For a comprehensive appreciation, the last experiment with zoomed final position is shown in Fig. 7. The asterisks '$*$' indicate the positions estimated by the proposed UWB localisation system. The dashed lines are the interpolation between the initial and final positions reached by the MR.

A set of measures can be appreciated near the corners, corresponding to the odometry reading when the robot makes the 90° turns. From the zoomed area it is feasible to determine that UWB navigation system offers commendable accuracy for MRs against the conventional odometry system. Furthermore, UWB system does not suffer from accumulated error as odometry does.

Table 2 shows that the final error between the initial position and the final robot position after three runs is 1 cm, an exceptional result for MR navigation. Comparing these results with those in Table 1, it is possible to determine that UWB navigation outperforms odometry navigation given appreciable accuracy enhancement.

The experiments demonstrate that the proposed navigation system using UWB as novel sensor technology can outperform classical approaches. The main advantage of the proposed system is that it does not depend on environment conditions such as temperature or illumination that affect classical sensor technology. Furthermore, it does not suffer from accumulated error since the localisation is absolute. Considering more accurate navigation systems such as stereo vision and laser sensor, it is possible to assert that UWB navigation attains accuracy levels similar to the aforementioned system with the advantage of low cost, low power and its intrinsic robustness, as previous work by the author reveals [24].

6 Conclusions

The experimental results demonstrate that developed UWB signal model, indoor channel model, transmitters, receiver and estimation algorithm integrate a complete localisation system that offers accurate position information for MR navigation. The statistical analysis shows that the UWB prototype evolving here, achieves prime positional accuracy since the 95% of the measurements result in errors below 20 cm. The UWB navigation clearly outperforms the odometry navigation and because of its absolute characteristics, avoids the problem of accumulated errors. The prototype used for experiments was built using commercial off-the-shelf components in agreement with the low-cost and low-power restrictions. An important characteristic of this developed prototype is that it can achieve optimal accuracy compared with commercial solutions, but with the great advantage of reduced cost. Furthermore, the software-defined radio concept considered in this work permits a changing the estimation and control algorithm during the system operation with minor effort. Finally, the system accuracy could be improved and the entire system cost and power consumption could be reduced if the complete receiver was integrated into a silicon chip.

7 Acknowledgments

The authors express their thanks to CONICET-Argentina; to the National University of San Juan, San Juan, Argentina; to the University of Southern California, Electrophysics-Department, California, USA, to National Instruments, and to Xilinx University Program for their financial support for this research.

8 References

1 Sharma, P., Krishnan, S., Zhang, G.: 'A multi-cell UWB-IR localization system for robot navigation'. Proc. IEEE Radio and Wireless Symp., Orlando, FL, 2008, pp. 851–854
2 González, J., Blanco, J.L., Galindo, C., *et al.*: 'Localización de vehículos combinando tecnología UWB y Gps en entornos interiores y exteriores'. Proc. XVIII Jornadas de Automatica, Huela, España, 2007
3 http://www.timedomain.com/
4 González, J., Blanco, J.L., Galindo, C., *et al.*: 'Mobile robot localization based on ultra-wide-band ranging: a particle filter approach', *Robot. Auton. Syst.*, 2009, **57**, pp. 496–507
5 Denis, B., Keignart, J., Daniele, N.: 'Impact of NLOS propagation upon ranging precision in UWB systems'. Proc. IEEE Conf. Ultra Wideband Systems and Technologies (UWBST'03), Reston, VA, November 2003, pp. 379–383
6 Lee, J.Y., Scholtz, R.A.: 'Ranging in a dense multipath environment using an UWB radio link', *IEEE J. Sel. Areas Commun.*, 2002, **20**, (9), pp. 1677–1683
7 Guvenc, I., Chong, C.-C., Watanabe, F., Inamura, H.: 'NLOS identification and weighted least-squares localization for UWB systems using multipath channel statistics', *EURASIP J. Adv. Signal Process.*, **2008**, pp. 1–14
8 Qi, Y., Kobayashi, H., Suda, H.: 'Analysis of wireless geolocation in a non-line-of-sight environment', *IEEE Trans. Wirel. Commun.*, 2006, **5**, (3), pp. 672–681
9 Senger, C., Kaiser, T.: 'BeamLoc – an approach for NLoS localization in UWB indoor environments'. IET Seminar on Ultra Wideband Systems, Technologies and Applications, London, UK, 20 April 2006, pp. 176–180
10 Segura, M., Mut, V., Patiño, D.: 'Wavelet correlation TOA estimation with dynamic threshold setting for IR-UWB localization system'. Proc. IEEE Latin American Conf. on Communication LATINCOM, Medellin, Colombia, September 2009, pp. 1–6
11 Progri, I.: 'Geolocation of RF signals: principles and simulations' (Springer Science & Business Media, LLC, 2011, 1st edn.)
12 Cramer, R.J.-M., Win, M.Z., Scholtz, R.A.: 'Evaluation of the multipath characteristics of the impulse radio channel'. Proc. IEEE Antennas and Propagation Society Int. Symp., 1998, vol. 2, pp. 864–868
13 Cassioli, D., Win, M.Z., Molisch, A.F.: 'The ultra-wide bandwidth indoor channel from statistical model to simulations', *IEEE J. Sel. Areas Commun.*, 2002, **20**, pp. 1247–1257
14 Molisch, A.F., Cassioli, D., Chong, C.-C., *et al.*: 'A comprehensive standardized model for ultrawideband propagation channels', *IEEE Trans. Antenna Propag.*, 2006, **54**, (11), pp. 3151–3166
15 Iida, S., Tanaka, K., Suzuki, H., *et al.*: 'A 3.1 to 5 GHz CMOS DSSS UWB transceiver for WPANs'. Proc. IEEE Int. Solid-State Circuits Conf., February 2005, vol. 48, pp. 214–215
16 Azakkour, A., Regis, M., Pourchet, F., Alquie, G.: 'A new integrated monocycle generator and transmitter for ultra-wideband (UWB)

communications'. Proc. IEEE Radio Frequency IC Symp., June 2005, pp. 79–82
17 Segura, M., Hashemi, H., Sisterna, C., Mut, V.: 'Experimental demonstration of self-localized ultra wideband indoor mobile robot navigation system'. Proc. IEEE Int. Conf. on Indoor Positioning and Indoor Navigation (IPIN), Zürich, Switzerland, 15–17 September 2010, pp. 1–9
18 Segura, M., Sisterna, C., Guzzo, M., Ensinck, G., Gil, C.: 'Ultra wideband digital receiver implemented on FPGA for mobile robot indoor self-localization'. Proc. IEEE VIII Southern Programmable Logic Conf., Cordoba, Argentina, 13–15 April 2011, pp. 97–102
19 Segura, M., Mut, V., Patiño, D.: 'Mobile robot self-localization system using IR-UWB'. Proc. IEEE Int. Workshop on Robotic and Sensors Environments (ROSE), Lecco, Italy, 6–9 November 2009, pp. 29–34
20 So, H.C., Hui, S.P.: 'Constrained location algorithm using TDOA measurements', *IEICE Trans. Fundam.*, 2003, **E86-A**, (12), pp. 3291–3293
21 Torrieri, D.J.: 'Statistical theory of passive location systems', *IEEE Trans. Aerosp. Electron. Syst.*, 1984, **AES-20**, (2), pp. 183–198
22 Chan, Y.T., Ho, K.C.: 'A simple and efficient estimator for hyperbolic location', *IEEE Trans. Signal Process.*, 1994, **42**, (8), pp. 1905–1915
23 Chung, W.C., Ha, D.S.: 'An accurate ultra wideband (UWB) ranging for precision asset location'. Proc. IEEE Conf. on Ultra Wideband Systems and Technologies, 2003, pp. 389–393
24 Segura, M., Auat Cheein, F.A., Toibero, M., Mut, V., Carelli, R.: 'Ultra wideband localization and SLAM: a comparative study for mobile robot navigation', *Sens. J. MDPI*, 2011, **11**, (2), pp. 2035–2055

doi: 10.1049/iet-rsn.2011.0352